Influence of internal viscosity on the large deformation and buckling of a spherical capsule in a simple shear flow

É. FOESSEL[2], J. WALTER[1], A.-V. SALSAC[1]
AND D. BARTHÈS-BIESEL[1]†

[1]Laboratoire de Biomécanique et Bioingénierie (UMR CNRS 6600),
Université de Technologie de Compiègne, BP 20529, 60205 Compiègne, France

[2]Ecole Polytechnique, 91128 Palaiseau, France

The motion and deformation of a spherical elastic capsule freely suspended in a simple shear flow is studied numerically, focusing on the effect of the internal-to-external viscosity ratio. The three-dimensional fluid–structure interactions are modelled coupling a boundary integral method (for the internal and external fluid motion) with a finite element method (for the membrane deformation). For low viscosity ratios, the internal viscosity no longer affects the capsule deformation. Conversely, for large viscosity ratios, the slowing effect of the internal motion lowers the overall capsule deformation; the deformation is asymptotically independent of the flow strength and membrane behaviour. An important result is that increasing the internal viscosity leads to membrane compression and possibly buckling. Above a critical value of the viscosity ratio, compression zones are found on the capsule membrane for all flow strengths. This shows that very viscous capsules tend to buckle easily.

Key words: capsule/cell dynamics, membranes

1. Introduction

A simple capsule consists of a liquid drop enclosed by a thin deformable elastic membrane. Capsules are ubiquitous particles widely used in the industry to protect active fragile products or in nature for the same purpose (cells, eggs and seeds). The mechanics of an initially spherical capsule freely suspended in a linear shear flow has received much attention over the years. It has been shown in particular that, because the internal volume is constant, when the capsule deforms, the enclosing membrane tends to buckle, as evidenced by the presence of negative (i.e. compressive) tensions in the membrane (Ramanujan & Pozrikidis 1998; Lac *et al.* 2004; Doddi & Bagchi 2008; Li & Sarkar 2008). This effect has been studied in detail for a viscosity ratio $\eta = 1$ between the internal and external liquid. It has been shown in particular that, for low shear strength, buckling occurs in the equatorial area of the capsule whereas for high shear strength, compression occurs in the vicinity of highly elongated and curved tips. The presence of compression is captured well by a membrane model

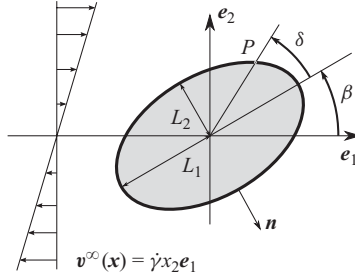† Email address for correspondence: dbb@utc.fr

FIGURE 1. The ellipsoid of inertia of the deformed capsule is used to evaluate the deformation: L_1 and L_2 are the two principal semi-diameters, β is the angle of the long axis with the far-field streamlines and δ defines the position of a point along the surface.

devoid of bending resistance, but the post-buckling behaviour cannot be computed with such a model.

The effect of the viscosity contrast $\eta \neq 1$ on the deformation of a spherical capsule has been mostly studied for two values $\eta = 0.2$ and $\eta = 5$ (Ramanujan & Pozrikidis 1998; Doddi & Bagchi 2008; Li & Sarkar 2008) with the recent addition of $\eta = 10$ (Bagchi & Kalluri 2010). However, the effect of η on the elastic tensions in the membrane and on the tendency towards buckling has never been studied.

It is the objective of this paper to show how the viscosity contrast influences the motion and deformation of a capsule suspended in a simple shear flow. The elastic tension distribution in the membrane will also be studied in detail, and we will show that the retarding effect of the internal liquid motion has a strong influence on the membrane mechanics. Indeed, for large-enough viscosity contrasts, it appears that the membrane is undergoing compression over half of its surface area.

In §2, the problem is briefly outlined. We then present the influence of the viscosity ratio on the capsule deformation and orientation and show the existence of two asymptotic regimes for low and high viscosity ratios. The elastic tension distribution in the membrane is then computed and the tendency towards buckling is discussed.

2. Problem statement and numerical method

We consider the deformation of a spherical liquid capsule of radius a, suspended in an unbounded fluid with viscosity μ. The capsule has a very thin membrane, treated as an isotropic hyperelastic surface S with surface shear modulus G_s and area dilation modulus K_s. The bending resistance is assumed to be negligible. The viscosity of the fluid inside the capsule is $\eta\mu$, and its density is equal to that of the surrounding fluid thus excluding gravity effects. The capsule is subjected to a simple shear flow with undisturbed flow velocity $v^\infty(x) = \dot{\gamma} x_2 e_1$, in a reference frame (O, e_1, e_2, e_3), centred on the capsule's centre and fixed with respect to the fluid at infinity. The capsule deforms until it reaches a steady profile while the membrane rotates around it (tank-treading motion). The deformation is measured by means of various geometric parameters that are evaluated on the ellipsoid of inertia of the deformed shape (figure 1):

(i) the Taylor parameter $D_{12} = (L_1 - L_2)/(L_1 + L_2)$ for the overall capsule deformation, where L_1 and L_2 are the half lengths of the two principal diameters of the ellipsoid of inertia in the shear plane;

(ii) the angle β for the inclination of the capsule's longest axis with respect to e_1;

70   (iii) the angle δ for the location of a capsule membrane material point in the shear
71 plane.
72   The two important non-dimensional parameters governing the capsule deformation
73 are the viscosity ratio η and the capillary number $Ca = \mu \dot{\gamma} a / G_s$, which measures
74 the relative importance of the viscous and elastic forces and can be considered as a
75 non-dimensional flow strength for a given capsule.
76   Assuming very small Reynolds number flows, the internal and external flows are
77 governed by the Stokes equations. The numerical modelling of the motion of a capsule
78 in a Stokes flow is now a classical problem (see, e.g. Pozrikidis 1992). Walter *et al.*
79 (2010) developed a numerical method to treat this problem that is based on the
80 coupling of a membrane finite-element method (for the capsule wall mechanics) and
81 a boundary integral method (for the internal and external flows). This method was
82 limited to the case when the two fluids had the same viscosity ($\eta = 1$). In the present
83 study, we extend it to cases when $\eta \neq 1$. We briefly outline the method focusing
84 mainly on the resolution technique used for the boundary integral equations when
85 $\eta \neq 1$. More details on the other steps of the procedure may be found in Walter *et al.*
86 (2010) and Barthès-Biesel, Walter & Salsac (2010).
87   The numerical procedure consists in following the position of the capsule material
88 points of the capsule membrane after the start of flow. At each time step, the position
89 of the membrane material points is thus known. The deformation of the capsule may
90 be computed, and the elastic tensions $\boldsymbol{\tau}$ are obtained from the values of the in-plane
91 stretch ratios λ_1 and λ_2. We use the law (Sk) proposed by Skalak *et al.* (1973), for
92 which the principal tensions are given by

$$\tau_1 = \frac{G_s}{\lambda_1 \lambda_2} \left[\lambda_1^2 (\lambda_1^2 - 1) + C(\lambda_1 \lambda_2)^2 ((\lambda_1 \lambda_2)^2 - 1) \right] \quad \text{(likewise for } \tau_2\text{).} \tag{2.1}$$

93 This law has independent values of G_s and K_s with $K_s / G_s = 1 + 2C$. Unless otherwise
94 stated, all the results given in the following sections correspond to the Sk law with
95 $C = 1$.
96   The finite-element method, used to solve the equilibrium of the membrane

$$\nabla_s \cdot \boldsymbol{\tau} + \boldsymbol{q} = \boldsymbol{0}, \tag{2.2}$$

97 provides the value of the load $\boldsymbol{q}$ exerted by the fluids on the membrane.
98   The boundary integral formulation for the three-dimensional motion of the internal
99 and external fluids can be written as

$$\boldsymbol{v}(\boldsymbol{x}) = \boldsymbol{v}^\infty(\boldsymbol{x}) - \frac{1}{8\pi\mu} \int_S \boldsymbol{J}(\boldsymbol{r}) \cdot \boldsymbol{q} \, \mathrm{d}S(\boldsymbol{y})$$
$$+ \frac{1-\eta}{8\pi} \int_S (\boldsymbol{v}(\boldsymbol{y}) - \boldsymbol{v}(\boldsymbol{x})) \cdot \boldsymbol{K}(\boldsymbol{r}) \cdot \boldsymbol{n}(\boldsymbol{y}) \, \mathrm{d}S(\boldsymbol{y}), \tag{2.3}$$

100 where $\boldsymbol{v}(\boldsymbol{x})$ is the velocity of the membrane point located at $\boldsymbol{x}$, and $\boldsymbol{r} = \boldsymbol{y} - \boldsymbol{x}$. The
101 Green kernels are given by

$$\boldsymbol{J}(\boldsymbol{r}) = \frac{1}{r}\boldsymbol{I} + \frac{\boldsymbol{r} \otimes \boldsymbol{r}}{r^3}, \quad \boldsymbol{K}(\boldsymbol{r}) = -6\frac{\boldsymbol{r} \otimes \boldsymbol{r} \otimes \boldsymbol{r}}{r^5}, \tag{2.4}$$

102 where $r = \|\boldsymbol{r}\|$ and $\boldsymbol{I}$ is the identity tensor. The implicit problem (2.3) is solved for $\boldsymbol{v}(\boldsymbol{x})$
103 by successive sub-iterations (denoted by the superscript n). As the procedure may not
104 converge if $\eta > 1$, we use a simple relaxation method

$$\boldsymbol{v}^{n+1}(\boldsymbol{x}) = \omega \boldsymbol{v}_s^{n+1}(\boldsymbol{x}) + (1 - \omega)\boldsymbol{v}^n(\boldsymbol{x}), \tag{2.5}$$
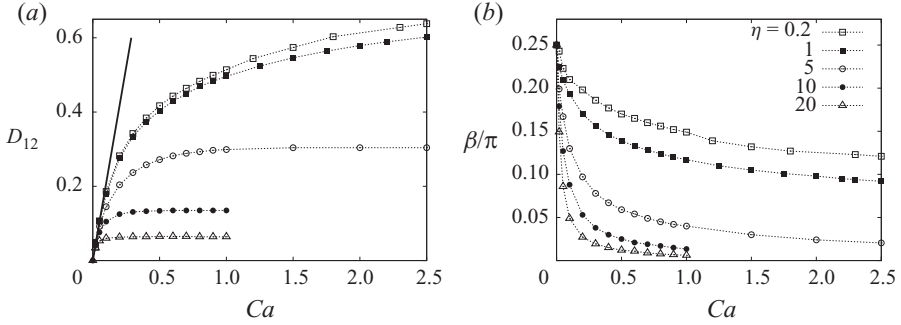
FIGURE 2. Steady-state value of (*a*) the Taylor parameter and (*b*) the inclination angle as a function of *Ca* for different values of η. In figure (*a*), the solid line represents the small-deformation theory (3.1).

where $v_s^{n+1}(x)$ is the left-hand side of (2.3) obtained by replacing $v(x)$ by $v^n(x)$ in the right-hand side of the equation. With a relaxation factor $\omega = 2/(1+\eta)$, this method is equivalent to that described by Pozrikidis (1992), but numerical tests show that using $\omega = 1.8/(1+\eta)$ significantly increases the convergence rate. The velocity is then integrated with an explicit second-order Runge–Kutta method to obtain the new position of the membrane points at the following time step. With this procedure, we were able to reproduce within 2 % the values of deformation D_{12} obtained for capsules with either an Sk or a neo-Hookean membrane and with $\eta = 0.2, 5, 10$ (Ramanujan & Pozrikidis 1998; Doddi & Bagchi 2008; Bagchi & Kalluri 2010).

3. Effect of the viscosity ratio and capillary number on the capsule deformation

The steady values of the deformation and inclination angle are presented in figure 2 as functions of *Ca* and η. The deformation D_{12} increases with *Ca* but decreases with η for a given value of *Ca*. The equilibrium shape of the capsule results from the balance between the jump in viscous stress across the membrane and the elastic load: $[\boldsymbol{\sigma}^{ext} - \boldsymbol{\sigma}^{int}] \cdot \boldsymbol{n} = \boldsymbol{q}$. For $\eta \ll 1$, the contribution of $\boldsymbol{\sigma}^{int}$ is small, and all the external stress is used to deform the membrane; thus D_{12} increases continuously with *Ca*. Furthermore, we find that when $\eta < 0.2$, the deformation curve is superimposed on the $\eta = 0.2$ curve, thus indicating that the internal flow is no longer important and that a low-viscosity asymptotic state has been reached.

As shown in figure 2(*a*), the deformation results are in good agreement with the small-deformation theoretical model of Barthès-Biesel & Rallison (1981), which is valid for $Ca \ll 1$:

$$D_{12} = \frac{25}{12}Ca + O(Ca^2), \quad \beta = \frac{\pi}{4} + O(Ca). \tag{3.1}$$

The range of validity of the first-order prediction decreases when η increases, although the deformation is smaller at high than at low viscosity ratios. This is due to the fact that this analysis is valid for $\eta = o(1/Ca)$, which reduces the capillary number range of validity when η increases.

For large values of η, the deformation reaches a plateau value when *Ca* increases (figure 2*a*). This result is consistent with the analysis of Barthès-Biesel & Rallison (1981) who also explored the case where the capsule deformation was limited by a high viscosity ratio ($\eta \gg 1$). They found that at the leading order, the deformation
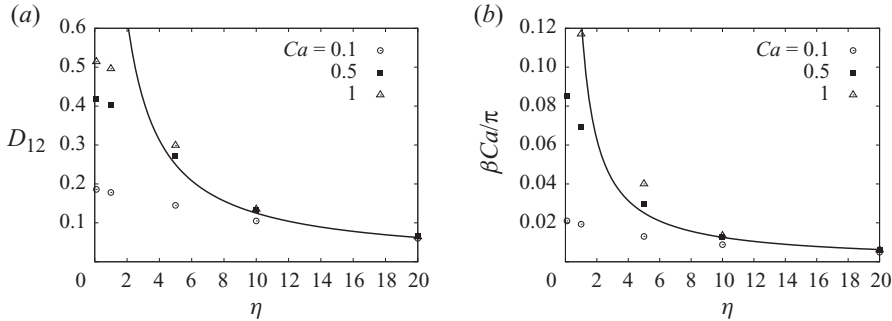
FIGURE 3. Steady-state value of (*a*) D_{12} and (*b*) βCa as a function of η for different values of Ca. The points represent the numerical results and the solid lines the small-deformation theory (3.2). The numerical results converge towards the asymptotic prediction for $\eta > 5$ and $Ca > 0.5$.

did not depend on Ca and that the orientation angle decreased with both Ca and η:

$$D_{12} = \frac{5}{4\eta} + O\left(\frac{1}{\eta^2}, \frac{1}{Ca\eta^2}\right), \quad \beta = \frac{15}{38 Ca\eta} + O\left(\frac{1}{\eta^2}, \frac{1}{Ca\eta^2}\right). \quad (3.2)$$

The deformation is plotted as a function of η in figure 3(*a*). It appears that when $\eta > 5$ and $Ca > 0.5$, the asymptotic theory gives a good prediction within 15 % for the deformation. The accuracy of the prediction (3.2) increases with η as expected.

The inclination angle results from the balance of two competing phenomena: the straining part of the external flow elongates the capsule in the $\mathbf{e}_1 + \mathbf{e}_2$ direction and thus sets β to $\pi/4$, whereas the vorticity rotates the capsule towards $\mathbf{e}_1$ and thus tends to decrease β to zero. Consequently, β decreases from $\pi/4$ as Ca increases. For low viscosity ratios, the flow inside the capsule does not affect the equilibrium-deformed shape much. This explains why the decrease of β with Ca is moderate (figure 2*b*). However, for highly viscous capsules that remain nearly spherical, the deformed shape results from the equal competition between the straining and rotational parts of the external simple shear flow in a fashion similar to the one observed for liquid drops (Rallison 1980). This results in a shape almost aligned with the streamlines in the asymptotic case where $\eta \gg 1$, as predicted by (3.2) and shown in figures 2(*b*) and 3(*b*).

4. Effect of the viscosity ratio on the membrane tensions

In order to analyse the effect of η on the membrane tensions, we consider the maximum value of the principal tensions τ_{max}, which is a good indicator of the risk of membrane mechanical failure, and the minimum value of the principal tensions τ_{min} whose sign determines the mechanical stability of the membrane. When τ_{min} is positive, the membrane is under tension everywhere and therefore stable, whereas when τ_{min} is negative, a part of the membrane is under compression and buckling occurs in the absence of bending resistance in the wall model.

Figure 4(*a*) shows the variation of τ_{max} as a function of Ca. As expected, τ_{max} increases with Ca. For a given capillary number, τ_{max} is also observed to decrease with the viscosity ratio η. This is a consequence of the decrease of the capsule deformation with η (figure 2*a*). The results can be collapsed onto a single curve for all the values of Ca and η, when one plots τ_{max} as a function of D_{12} (Figure 4*b*). This is due to the fact that, for a given membrane-constitutive law, the capsule elongation (and thus deformation) determines the elastic stress in the membrane. A
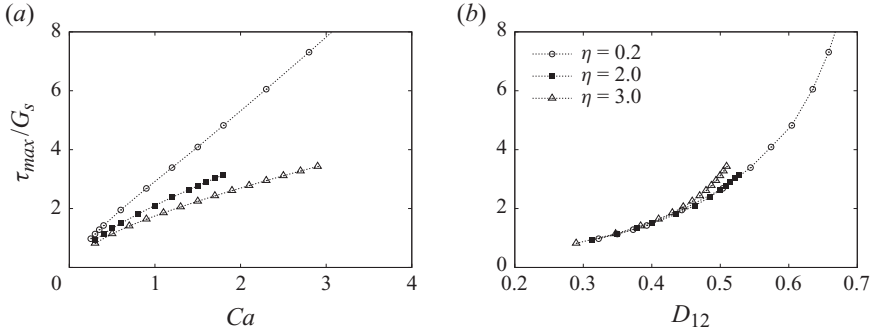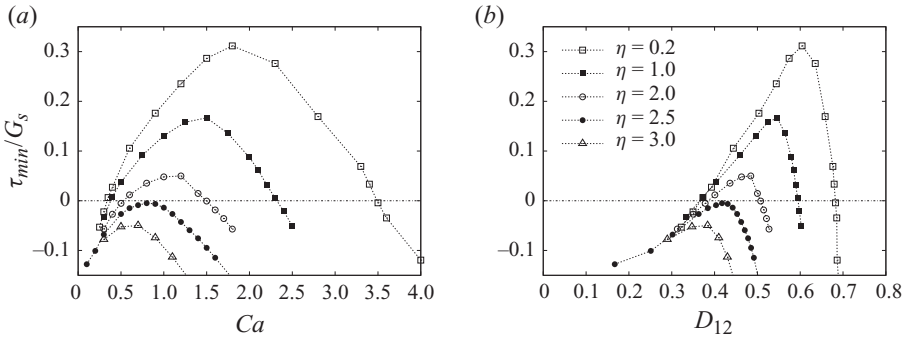
FIGURE 4. Maximum value of principal tensions as a function of (*a*) Ca and (*b*) D_{12}.

FIGURE 5. Minimum value of principal tensions as a function of (*a*) the capillary number and (*b*) the Taylor parameter.

small departure from the general curve is found for higher viscosity ratios at large deformation. This may be due to buckling effects, which are discussed in the next section.

The values of τ_{min} show the existence of two different types of behaviour (figure 5*a*). For low and moderate values of η, there exists a range of capillary numbers for which $\tau_{min} > 0$: the membrane is under tension and thus mechanically stable. We denote Ca_L and Ca_H as the two critical capillary numbers defined by $\tau_{min}(Ca_L) = \tau_{min}(Ca_H) = 0$, $Ca_L \leqslant Ca_H$. Such findings concur with those of Lac *et al.* (2004) for $\eta = 1$. However, for viscosity ratios above a critical value η_c ($\eta_c \approx 2.5$), we find that the membrane is always undergoing compression somewhere.

4.1. *Low shear compression*

When $Ca < Ca_L$, the initially spherical capsule is extended by the flow in the β-direction. The capsule being a closed shape with a constant volume is thus compressed along the equator and tends to buckle in this area as shown in figure 6(*a*). As Ca and the capsule deformation increase, the isotropic part of the tensions in (2.1), related to the area dilation modulus K_s, increases too and eventually becomes large enough to overcome compressive effects for $Ca = Ca_L$. This phenomenon depends only on the capsule extension (and thus D_{12}) and is independent of η. Consequently, if τ_{min} is plotted as a function of D_{12}, Ca_L occurs at roughly the same value of the Taylor parameter $(D_{12})_L = 0.37$ (figure 5*b*). For $Ca \gtrsim Ca_L$, the minimum tension τ_{min} is positive so that the membrane is under tension everywhere.
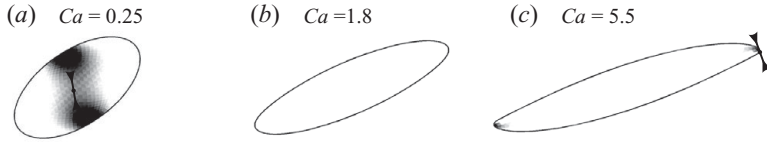
FIGURE 6. Location of negative tensions for $\eta = 0.2 < \eta_c$. The capsule is shown in the shear plane (e_1, e_2). White areas are taut; where negative tensions occur, their intensity is represented by the grey scale. Arrows show the general direction of compression.
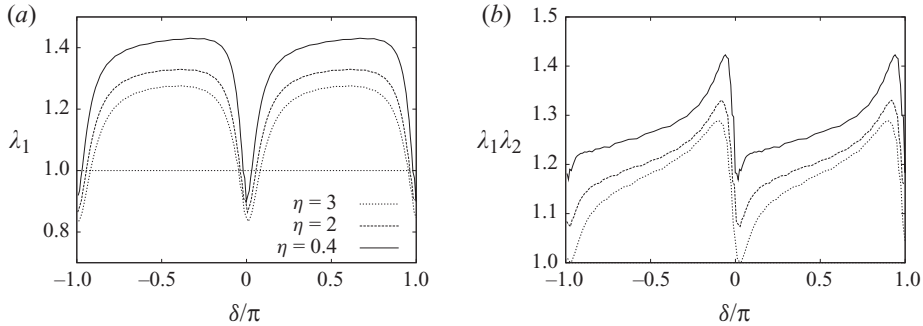

FIGURE 7. Stretch ratio λ_1 and surface extension ratio $\lambda_1\lambda_2$ along the capsule profile in the shear plane at different viscosity ratios for $Ca = 1.5$, using Sk law $(C = 1)$.

4.2. *High shear compression*

As Ca increases further, τ_{min} starts to decrease and eventually becomes negative. Contrary to the previous case, this decrease is linked to the appearance of a compression zone now located near the tip of the capsule. In order to explain this phenomenon, we study the intersection of the capsule surface with the shear plane (a principal direction of strain in view of the problem symmetry) and measure its elongation λ_1. The second principal elongation λ_2 is measured in the direction normal to the shear plane. The membrane velocity varies along the interface, being maximum on the short axis and minimum on the long axis (i.e. at the tip) in a fashion analogous to the surface velocity field proposed by Keller & Skalak (1982). Correspondingly, the principal membrane elongation λ_1 in the shear plane is maximum on the capsule equator and minimum at the tip (defined by $\delta = 0$), as shown in figure 7, where λ_1 is plotted as a function of δ. Values of $\lambda_1 < 1$ at the tips do not necessarily mean that the membrane is undergoing compression. Indeed, if the ratio of the deformed to the underformed surface areas $\lambda_1\lambda_2$ is large enough, the resistance to area increase can balance the decrease in λ_1 in (2.1) so that no negative tensions appear. This is illustrated in figure 7 where the variations of λ_1 and $\lambda_1\lambda_2$ along the capsule profile in the shear plane are plotted for $Ca = 1.5$ and three different values of η. For $\eta = 0.4$, $Ca = 1.5$ falls into the interval $[Ca_L; Ca_H]$; the membrane is under tension and the area change at the tip is large enough to compensate the decrease of λ_1. For $\eta = 2$, $Ca = 1.5$ is just below Ca_H, and the area dilation just balances the decrease in λ_1. Finally, for $\eta = 3$, there is no $[Ca_L; Ca_H]$ interval. The area change cannot compensate the decrease of λ_1 at the tips, as it is equal to zero: the membrane is undergoing compression at these locations.

The fact that Ca_H decreases with η (figure 5a) is due to the lower deformation, and correspondingly lower area dilation, of a viscous capsule. However, the global
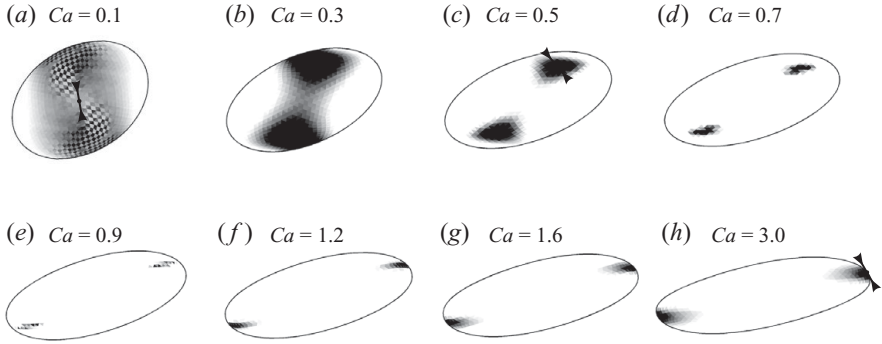
(*a*) *Ca* = 0.1   (*b*) *Ca* = 0.3   (*c*) *Ca* = 0.5   (*d*) *Ca* = 0.7

(*e*) *Ca* = 0.9   (*f*) *Ca* = 1.2   (*g*) *Ca* = 1.6   (*h*) *Ca* = 3.0

FIGURE 8. Location of negative tensions for $\eta = 2.5 \gtrsim \eta_c$. Same legend as in figure 6.
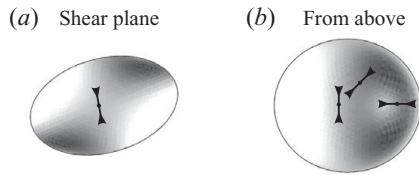
(*a*)   Shear plane   (*b*)   From above

FIGURE 9. Location of negative tensions for $\eta = 5$ and $Ca = 0.3$. Same legend as in figure 6.

deformed shape of the capsule is not enough to determine the local deformation distribution. Therefore, Ca_H does not depend solely on the geometry as Ca_L did, which indicates that three-dimensional effects play an essential role in the buckling phenomena.

   The present explanation for the formation of compression zones near the tips of the capsule differs from the assumption formulated by Lac *et al.* (2004). They had interpreted it as a consequence of the twisting couple induced by the flow vorticity when capsules were highly elongated and showed twisted capsule profiles obtained for values of Ca well above Ca_H. But if the torsion of the profile were the only phenomenon, Ca_H would have corresponded to a value of D_{12} independent of η, which is clearly not the case as shown in figure 5(*b*).

4.3. *High viscosity ratios*

The two limits Ca_L and Ca_H correspond to two different compression phenomena. Indeed, when $\eta < \eta_c$, as Ca is increased from zero, the capsule is first under compression in the equatorial region, then fully stretched everywhere and finally under compression at the tips as shown in figure 6. This is consistent with the results obtained for $\eta = 1$ (Lac *et al.* 2004; Walter *et al.* 2010). However, close to η_c, Ca_L tends towards Ca_H, which indicates that both phenomena coexist at high viscosity ratios and that their effects add up. Figure 8 shows that, for η just above the critical viscosity ratio η_c, negative tensions never subside as Ca is increased, but migrate from the equatorial zone to the tips while changing direction. At even higher viscosity ratios, the two phenomena occur at the same time: negative tensions occur both at the tips and in the equatorial plane, evolving continuously from an 'equatorial' to an 'axial' orientation (figure 9).

   The interaction with Ca_H may influence the value of Ca_L when η is only slightly below η_c. We note that the given interpretation of the compression phenomenon

related to Ca_L should create negative tensions uniformly distributed in the equatorial zone. However, figure 8 shows that during the migration, the negative tensions are no longer located in the shear plane. We find that this behaviour is true even when $\eta \lesssim \eta_c$: negative tensions start to migrate but subside before reaching the tip. Therefore, when η is only slightly below η_c, the compression phenomenon related to Ca_H interacts with the equatorial compression related to Ca_L. This explains why $(D_{12})_L$ is slightly different in this case from the common value found for lower viscosity ratios (figure 5*b*).

5. Conclusion

The internal viscosity of a spherical capsule freely suspended in a simple shear flow plays an important role on the capsule deformation and on the resulting elastic tensions in the membrane.

An interesting new result of this study concerns the elastic tensions in the membrane. We find that increasing the internal viscosity leads to membrane compression and possible buckling for all shear strengths when $\eta > \eta_c$. We have also shown that the compression at the capsule tips is due to the slowing down of the membrane rather than a viscous torsion couple. Highly viscous capsules exhibit large areas with negative tensions. It must be noted that, while the present model remains stable enough to determine the location of these areas, a model taking into account the bending stiffness of the membrane would be more appropriate for such capsules.

All the results in this paper correspond to a membrane following the Sk law with $C = 1$. Computations were also conducted with the neo-Hookean law (NH; see, for example, Barthès-Biesel, Diaz & Dhenin 2002) but are not shown here. When $C = 1$, the Sk and NH laws share the same small-deformation behaviour, but the Sk law is strain-hardening under large deformation, whereas the NH law is strain-softening. As a consequence, an NH capsule deforms more readily than an Sk capsule: for example, the deformation of an NH capsule is about 0.69 for $Ca = 1$ and $\eta = 0.2$, while it is about 0.5 for a capsule with an Sk membrane under the same conditions.

Capsules with a membrane obeying either the Sk or the NH law have a qualitatively similar behaviour with respect to the viscosity ratio. In particular, the deformation obtained for $\eta = 0.2$ also represents a limit for the deformation of any lower viscosity capsule and is about 12 % higher than the deformation obtained for $\eta = 1$. Some quantitative differences exist between capsules with an NH or Sk membrane. The value of $(D_{12})_L$ for the NH law is larger than that for the Sk law (0.45 vs. 0.37). This is due to the nonlinear behaviour of the laws: when undergoing uniaxial traction with a given stretch ratio, the *effective* area dilation modulus is smaller for an NH membrane than for an Sk membrane. The NH capsule therefore needs to be more elongated for the negative tensions to subside at the equator. We also find that, for a given $\eta < \eta_c$, the value of Ca_H is significantly lower for the NH law, which is consistent with the findings of Lac *et al.* (2004) at $\eta = 1$. As a consequence, η_c is lower for the NH law (1.25 vs. 2.5). Thus, the NH law behaves qualitatively like the Sk law with $C = 1$, but the shear-thinning behaviour of this law causes negative tensions and buckling to be much more prevalent.

On the practical side, for experimental or numerical studies of spherical capsules, some points are worth mentioning:

(i) For viscosity ratios $\eta \geqslant 1$, the slowing effect of the internal motion lowers the overall capsule deformation. An asymptotic state is reached for highly viscous capsules ($\eta > 5$), with a deformation given by $D_{12} = 5/4\eta$ irrespective of the flow

strength and the membrane-constitutive law. Such capsules are expected to exhibit large compression zones, which would be very interesting to study experimentally.

(ii) A viscosity ratio $\eta = 0.2$ seems to be representative of all low-viscosity capsules with $\eta \ll 1$, as regards deformation and orientation. Furthermore, D_{12} for $\eta \leqslant 0.2$ is only approximately 10 % larger than for $\eta = 1$, with a difference in orientation of about 20 %. Consequently, one may reasonably consider using results obtained for $\eta = 1$ to model any lower viscosity ratio.

(iii) The previous point is an important finding for experimental studies of capsules. Indeed, experiments are generally performed in a very viscous outer fluid so as to reach large deformations at moderate shear rates. This leads to very small values of η; for instance, Chang & Olbricht (1993) worked with $\eta \in [0.004, 0.08]$ and Walter, Rehage & Leonhard (2000) reported results corresponding to $\eta = 0.001$.

(iv) These findings are also important for numerical studies because the computation time increases steeply with $|\eta - 1|$ as compared to the case $\eta = 1$.

REFERENCES

BAGCHI, P. & KALLURI, R. M. 2010 Rheology of a dilute suspension of liquid-filled elastic capsules. *Phys. Rev.* E **81**, 056320.

BARTHÈS-BIESEL, D., DIAZ, A. & DHENIN, E. 2002 Effect of constitutive laws for two dimensional membranes on flow-induced capsule deformation. *J. Fluid Mech.* **460**, 211–222.

BARTHÈS-BIESEL, D. & RALLISON, J. M. 1981 The time-dependent deformation of a capsule freely suspended in a linear shear flow. *J. Fluid Mech.* **113**, 251–267.

BARTHÈS-BIESEL, D., WALTER, J. & SALSAC, A.-V. 2010 Flow-induced deformation of artificial capsules. In *Computational Hydrodynamics of Capsules and Biological Cells*. pp. 35–70. Taylor & Francis.

CHANG, K. S. & OLBRICHT, W. L. 1993 Experimental studies of the deformation and breakup of a synthetic capsule in steady and unsteady simple shear flow. *J. Fluid Mech.* **250**, 609–633.

DODDI, S. K. & BAGCHI, P. 2008 Lateral migration of a capsule in a plane Poiseuille flow in a channel. *Intl J. Multiphase Flow* **34** (10), 966–986.

KELLER, S. R. & SKALAK, R. 1982 Motion of a tank-treading ellipsoidal particle in a shear flow. *J. Fluid Mech.* **120**, 27–47.

LAC, É., BARTHÈS-BIESEL, D., PELEKASIS, N. A. & TSAMOPOULOS, J. 2004 Spherical capsules in three-dimensional unbounded Stokes flow: effect of the membrane constitutive law and onset of buckling. *J. Fluid Mech.* **516**, 303–334.

LI, X. & SARKAR, K. 2008 Front tracking simulation of deformation and buckling instability of a liquid capsule enclosed by an elastic membrane. *J. Comput. Phys.* **227** (10), 4998–5018.

POZRIKIDIS, C. 1992 *Boundary Integral and Singularity Methods for Linearized Viscous Flow*. Cambridge University Press.

RALLISON, J. M. 1980 Note on the time-dependent deformation of a viscous drop which is almost spherical. *J. Fluid Mech.* **98**, 625–633.

RAMANUJAN, S. & POZRIKIDIS, C. 1998 Deformation of liquid capsules enclosed by elastic membranes in simple shear flow: large deformations and the effect of capsule viscosity. *J. Fluid Mech.* **361**, 117–143.

SKALAK, R., TOZEREN, A., ZARDA, R. P. & CHIEN, S. 1973 Strain energy function of red blood cell membranes. *Biophys. J.* **13**, 245–264.

WALTER, A., REHAGE, H. & LEONHARD, H. 2000 Shear-induced deformation of polyamide microcapsules. *Colloid Polym. Sci.* **278**, 169–175.

WALTER, J., SALSAC, A.-V., BARTHÈS-BIESEL, D. & LE TALLEC, P. 2010 Coupling of finite element and boundary integral methods for a capsule in a Stokes flow. *Intl J. Numer. Meth. Engng* **83**, 829–850.